Int. J. Multiphase Flow Vol. 15, No. 5, pp. 787–802, 1989
Printed in Great Britain. All rights reserved

0301-9322/89 $3.00 + 0.00
Copyright © 1989 Pergamon Press/Elsevier

AN AXIAL VIEWING PHOTOGRAPHIC TECHNIQUE TO STUDY TURBULENCE CHARACTERISTICS OF PARTICLES

M. M. LEE,[1] T. J. HANRATTY[1] and R. J. ADRIAN[2]

Departments of [1]Chemical Engineering and [2]Theoretical and Applied Mechanics, University of Illinois, Urbana, IL 61801, U.S.A.

(*Received* 3 *August* 1988; *in revised form* 15 *March* 1989)

Abstract—An axial viewing photographic technique has been developed which can study the turbulence characteristics of droplets in planes perpendicular to the direction of mean flow. The technique provides direct measurements of particle flux and provides measurements of the mean-square values of both the r- and θ-components of turbulent velocity fluctuations of the droplets. Results are given which show the influence of particle inertia on droplet turbulence for droplets injected into a fluid flowing turbulently in a pipe.

Key Words: two-phase flow, droplet diffusion, turbulence, photographic techniques

INTRODUCTION

Particles or droplets contained in a fluid flowing turbulently in a vertical pipe will attain a random motion because of the influence of the turbulent velocity fluctuations. This paper describes an optical technique that has been developed to study this motion, and presents initial results with this technique.

The motivation is to obtain an understanding of the rate of deposition of droplets on the wall, which is usually described by the rate equation

$$R_D = k_D \langle C \rangle, \tag{1}$$

where R_D is the rate of deposition per unit area, $\langle C \rangle$ is the bulk-averaged concentration of droplets and k_D is the deposition constant. If the droplets have been in the field long enough for their method of introduction to be ignored, k_D will be related entirely to the turbulence characteristics of the drops.

If the drops are small enough they will completely follow the fluid turbulence, so that the mean-squares of the turbulent velocity fluctuations, $\overline{v_i^2}$, are equal to the fluid values, $\overline{u_i^2}$. This will not be the case for larger drops. A parameter characterizing the ability of a drop to follow the fluid turbulence is the inverse time constant,

$$\beta = \frac{3 C_D \rho_f}{4 d_p \rho_p} |U_r|, \tag{2}$$

where C_D is the drag coefficient, ρ_f is the density of the fluid, ρ_p is the density of the particle, d_p is the particle diameter and $|U_r|$ is the relative velocity between the particle and the fluid. For particle Re values small enough that C_D is given by Stokes' law,

$$\beta = \frac{18 \mu_f}{\rho_p d_p^2}, \tag{3}$$

where μ_f is the fluid viscosity. The product of $\beta^{-1} = \tau$ and the velocity of a particle gives the stopping distance of a particle in a stagnant fluid.

Measurements of k_D can be classified by using the dimensionless group, $\tau^+ = u^{*2}/\nu_f \beta$ (McCoy & Hanratty 1977). This paper is concerned with situations in which τ^+ is sufficiently large that the stopping distance is much greater than the thickness of the viscous wall region and that the non-homogeneities of the turbulence can be ignored.

Theoretical treatments for $\tau^+ > 20$ have been given by Friedlander & Johnstone (1957), Hutchinson *et al.* (1971) and Ganic & Mastanaiah (1981). All of these approaches have used diffusional models. The principal differences are in the treatment of the boundary condition at the wall. All of these studies emphasize the need to predict $\overline{v_i^2}$ and the particle diffusivity, ϵ_p, so that the main impediment in establishing a theory is the lack of laboratory measurements. The technique described in this paper was developed to address this need.

The system studied was the downward flow of air in a 5.08 cm pipe. Droplets of uniform size were injected into the center of the pipe at a velocity approximately equal to that of the air. The cross section of the pipe was illuminated by electronic flash units at several locations downstream of the point of injection. A camera at the bottom of the pipe views upward into the pipe and captures images of particles in an illuminated cross section. By synchronizing the flashes with the mean translation of the drops, images of the same particles can be obtained as they move down the pipe. The analysis of these photographs gives the radial and tangential components of the velocities of the particles. The mean-squares of the fluctuations in these two measurements give a measure of how well the particles follow the turbulence. The mean of the radial velocity component, $\bar{v}_r$, gives a direct measurement of the flux, $\bar{N}(r)$, at a given radial location if the mean concentration $\bar{C}(r)$ is known, since

$$\bar{N} = \bar{v}_r \bar{C}. \qquad [4]$$

The Eulerian diffusion coefficient can be calculated from these measurements since

$$\epsilon_p(r) = \frac{\bar{N}}{\left(-\frac{d\bar{C}}{dr}\right)}. \qquad [5]$$

Laser-Doppler velocimetry has been used to measure axial velocity components by using beams that enter the system through the pipe wall. The interesting aspect of the work described in this paper is that axial viewing filters out the much larger axial flow component so that velocities in planes perpendicular to the flow direction can be measured more easily. The idea of using axial view photography was motivated by the works of Arnold & Hewitt (1967) and Hewitt & Roberts (1969); however, the implementation of this idea here is significantly different from this previous work done at Harwell Laboratory (Oxon., U.K.).

DESCRIPTION OF THE EXPERIMENTS

Flow system

A schematic of the system in which the experiments were performed is shown in figure 1. The air flowing to the pipe was humidified to 60–70% so as to keep the evaporation of the droplets as small as possible. The droplets were injected into the center of the pipe 90 pipe dia from the inlet.

A detailed description of the droplet injector system is given in recent papers by Vames & Hanratty (1988) and Lee & Hanratty (1988). The droplets were formed from water that was deionized and further purified by the Sybron/Barnstead Nanopure system at a resistivity of $18.3 \times 10^6\,\Omega$-cm to filter out contaminants of $<0.2\,\mu$m. A PZT-5H Bimorph piezoelectric tranducer introduced periodic disturbances to the water before it was fed to a right-angled 3.18 mm o.d. stainless steel tube. These disturbances caused the liquid jet issuing from the injector orifice to break up into a stream of droplets of uniform diameter.

The orifice, developed by Lee (1984), consists of a thin cross section of a glass capillary tube fastened to the end of the stainless steel injector with adhesive. The glass was ground to a thickness of <1 mm to minimize pressure losses and polished on both sides so that the edges of the orifice were smooth. The glass capillaries used in this study had i.d.s 25.4, 50.8 and 76.2 μm. These produced steady streams of droplets of 50, 90 and 150 μm directed downward in a direction perpendicular to the plane containing the tip.

The light sheets were formed by an electronic flash unit and a spherical copy lens. The flash units were Nissin 4000 GW with thyristor auto/bounce double reflector and xenon tubes. A 180 μs light pulse was selected to satisfy the needs of light intensity and short pulse width to avoid any streaky

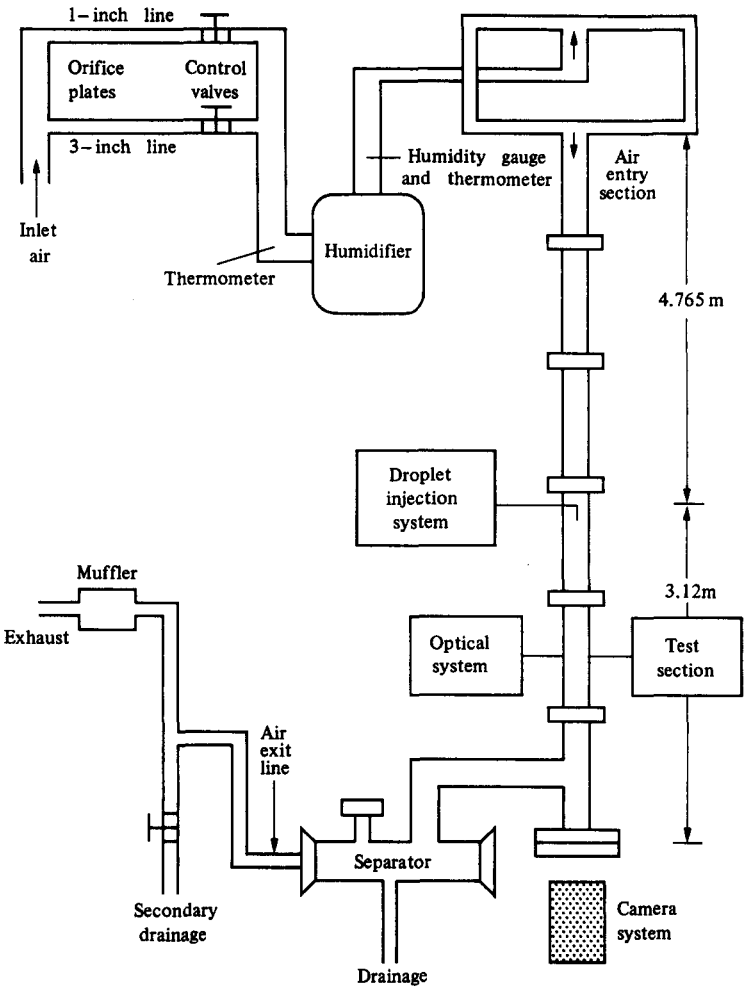

Figure 1. Schematic of the flow systems.

droplet images. Kodax Tri-X ASA 400 black-and-white film was chosen as a compromise of the requirements of fast film speed and high resolution (minimal graininess).

The electronic flash units, used in the optical experiments, were fastened on a horizontal aluminum platform which could be located at any distance downstream from the injector.

The camera was situated on a three-dimensional traversing mechanism at the bottom of the pipe. A camera viewing port, which allowed the air to leave through the side, was attached to the end of the test section. An optically flat quartz window was used for the viewing of the camera. In order to prevent excessive accumulation of water droplets, a protection shield was installed above this window. During the actual photo-taking process, the protection shield was manually removed for approx. 1 s to allow a clear view of the object plane for the camera. The minute amount of water deposited on the quartz window during this period of 1 s evaporated before the next shot was taken.

Optical system

A sketch depicting the optical measurements is given in figure 2. The five parallel light sheets were 1 cm thick and located adjacent to one another. The distance between the camera lens and the light sheets was about 100 cm.

The delay time between flashes was determined from a calculation of the axial velocity of the droplets. A capture efficiency, defined as the fraction of the observed trajectories for which the number of images equals the number of light sheets, varied between 63 and 83%. In order to

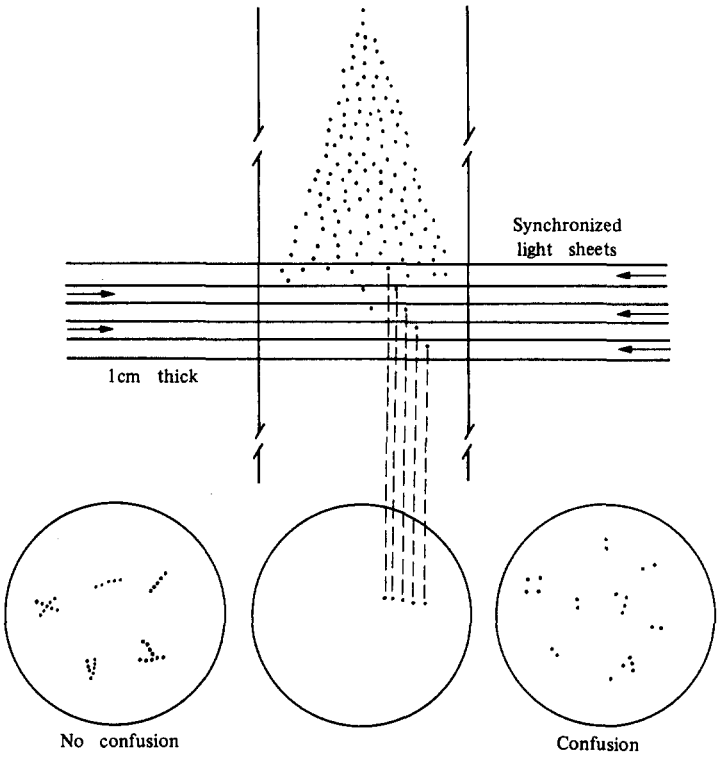

Figure 2. Axial viewing photographic technique.

minimize biasing errors, all trajectories with two or more images were included in the data bank. By doing this, 95% of the trajectories were captured.

The experiments were performed in a completely darkened room. The aperture of the camera was open during the multiple light pulses, and multiple images were superimposed on a single photograph. As a result, the trajectory of a single droplet could be clearly identified on the photographic film. If only two light sheets had been used, a potential problem could arise in identifying correct pairing if the paths of the droplets cross each other. Therefore, multiple light sheets, three or more, were used to avoid this possible confusion. This technique also identified the direction of the droplet paths by "defocusing" the images in the very last light sheet so that the blurred image in a set of images denoted the end of the trajectory. Since it was only necessary to locate the center of each droplet image, these blurred images could be used as data points as well as markers. A typical photograph of the droplet images is shown in figure 3.

A semi-automatic digitizing technique was employed to digitize these droplet images on Cartesian coordinates. The velocity components, x- and y- were determined from the distance between two successive images and the time delay between two adjacent flashes. Then, using a coordinate transformation, the radial and tangential velocity components of the droplets were obtained.

The manually operated digitizer was a Mitutoyo PJ311 profile projector, consisting of a $10\times-50\times$ zoom lens, a cross travel stage, two micrometer-heads for the x- and y-directions, and a digital readout GS-counter. A computer was used to interface the data transfer as well as to the process the data.

A small fraction of the droplets which had very low radial velocities created a streak-like pattern, due to overlapping of the droplet images. The locations of two points were estimated as being one radius away from the edges of the head and the tail of the streak. The distance between these two points, ΔL, was the droplet displacement within a given time frame. Since one cannot identify how many images were within that streak, the assumption was made that exposures from all light sheets were obtained on the film. Although this treatment was not exact, it involved only a small fraction, about 10%, of the total number of droplets.

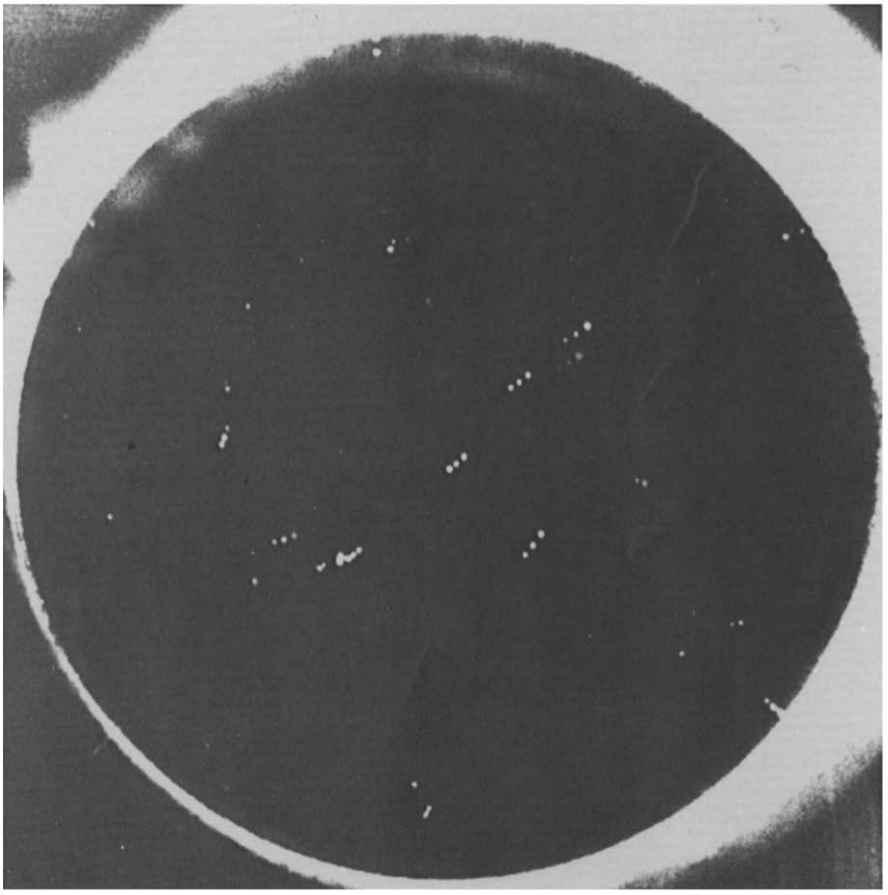

Figure 3. Photograph of the droplet trajectories for the 150 μm droplets.

Data treatment

The velocity components of a droplet in the x- or y-direction were determined from the negative as

$$V_{x,j,\text{image}} = \frac{(X_{j+1} - X_j)}{(\mathrm{d}t \times M)} \quad [6]$$

and

$$V_{y,j,\text{image}} = \frac{(Y_{j+1} - Y_j)}{(\mathrm{d}t \times M)}, \quad [7]$$

where dt is the time delay between two adjacent flash units, M is the magnification of the droplet image on the photographic negative and x_j and y_j represent the location of the jth image of a droplet on the negative.

The average velocity, v_x and v_y, for the jth droplet trajectory was calculated from

$$V_{x,j,\text{image}} = \frac{1}{n}\sum_{i=1}^{n} V_{x,j,\text{image}} \quad \text{and} \quad V_{y,j,\text{image}} = \frac{1}{n}\sum_{i=1}^{n} V_{y,j,\text{image}}, \quad [8]$$

where the $n = 2$ when three light sheets are used and $n = 3$ when four light sheets are used.

An important correction was needed to obtain the correct droplet velocities because of the effect of perspective in the optics. Figure 4 shows how images in the object plane are projected onto the image plane, i.e. the photographic negative, assuming that the center of the lens is in perfect alignment with the pipe center. It is clear from figure 4 that even if the droplets move axially without any radial velocity, the image projected onto the negative would still exhibit a radial displacement. The amount of this apparent radial displacement increases as the droplet approaches the pipe wall.

This perspective distortion arises because the distance from the optical lens to the object plane, d_o, is comparable with the distance to the image plane, d_i. If $d_o \gg d_i$, this error would be negligible. The magnification of the images also changes by approx. 4% from the first light sheet to the fifth light sheet. A correction for this distortion can be made as follows.

Let

$$\mathbf{x} = \text{a two-dimensional vector, } (x, y), \text{ in the object plane}$$

and

$$\mathbf{X} = \text{a two-dimensional vector, } (X, Y), \text{ in the image plane.}$$

Then,

$$\mathbf{X} = -M(z)\mathbf{x}, \tag{9}$$

where M is the magnification. Letting $M_0 = d_i/d_o$ be the magnification of particles lying in the object plane of the lens, and z be the displacement out of this plane, it follows that

$$M(z) = \frac{M_0}{\left(1 - \frac{z}{d_o}\right)}. \tag{10}$$

Taking the differential of [9] and [10],

$$\mathrm{d}\mathbf{X} = -M(z)\,\mathrm{d}\mathbf{x} - \mathbf{x}\,\mathrm{d}M(z) \tag{11}$$

and

$$\mathrm{d}M(z) = \frac{M^2(z)}{M_0 d_o}\,\mathrm{d}z \cong \frac{M_0}{d_o}\,\mathrm{d}z. \tag{12}$$

Substituting [12] into [11] and dividing by $\mathrm{d}t$ results in

$$\frac{\mathrm{d}\mathbf{X}}{\mathrm{d}t} = -M_0\left(\frac{\mathrm{d}\mathbf{x}}{\mathrm{d}t} + \frac{\mathbf{x}}{d_o}\frac{\mathrm{d}z}{\mathrm{d}t}\right). \tag{13}$$

Now rearranging and expressing in individual components,

$$\frac{\mathrm{d}x}{\mathrm{d}t} = -\frac{1}{M(z)}\frac{\mathrm{d}X}{\mathrm{d}t} + \frac{X}{d_o M_0}\frac{\mathrm{d}z}{\mathrm{d}t} \tag{14}$$

and

$$\frac{\mathrm{d}y}{\mathrm{d}t} = -\frac{1}{M(z)}\frac{\mathrm{d}Y}{\mathrm{d}t} + \frac{Y}{d_o M_0}\frac{\mathrm{d}z}{\mathrm{d}t}. \tag{15}$$

In [14] and [15] $\mathrm{d}z/\mathrm{d}t$ is the axial velocity of the droplets. It can be approximated by

$$\frac{\mathrm{d}z}{\mathrm{d}t} = \bar{U} + v_T, \tag{16}$$

where $\bar{U}$ is the mean axial fluid velocity and v_T is the terminal velocity of the droplets in a quiescent fluid. For simplicity, $\bar{U}$ was estimated from the seventh power law:

$$\bar{U} = \bar{U}_{\max}\left(\frac{R - r}{R}\right)^{1/7}, \tag{17}$$

where $r = 0$ at the pipe center. The second terms on the r.h.s. of [14] and [15] represent the "fictitious" radial velocity due to the perspective distortion.

INTERPRETATION

Two parameters can be identified as defining the principal influences of system variables on the ability of the particles to follow fluid turbulence. One of these represents the inertial effects of the

particles; it is given as the ratio of a time constant of the fluid turbulence to the particle time constant, $\beta\tau_{Lf}$. Here, the fluid time constant is given as the Lagrangian time scale,

$$\tau_{Lf} = \int_0^\infty R_{Lf}(\theta)\, d\theta, \qquad [18]$$

where R_{Lf} is the Lagrangian correlation coefficient of the fluid particles.

The second parameter is a measure of the "crossing trajectory effect" first identified by Yudine (1959). It is defined as the ratio of the free fall terminal velocity of the particles to the magnitude of the velocity fluctuations, v_T/q, where

$$q^2 = \tfrac{1}{2}(\overline{u_r^2} + \overline{u_\theta^2}). \qquad [19]$$

For the case of a linear drag law the following relations can be derived between the particle and fluid turbulence for a particle that has been in an isotropic field for a long time [see [13] and [26] of Friedlander (1957)]:

$$\epsilon_p = \overline{u^2} \int_0^\infty R_f(\theta)\, d\theta \qquad [20]$$

and

$$\overline{v^2} = \overline{u^2}\beta \int_0^\infty e^{-\beta\theta} R_f(\theta)\, d\theta. \qquad [21]$$

The correlation $R_f(\theta)$ is different from the usual Eulerian or Lagrangian correlation coefficients. It represents the correlation of the fluctuating fluid velocity seen by a probe (the particle) moving in an unknown path through the fluid. The main theoretical problem is the prediction of the relation of $R_f(\theta)$ to measurable statistical properties of the fluid turbulence. If it is represented by

$$R_f(\theta) = e^{-\alpha\theta}, \qquad [22]$$

then

$$\overline{v^2} = \overline{u^2}\left(\frac{\beta}{\alpha + \beta}\right) \qquad [23]$$

and

$$\epsilon_p = \frac{\epsilon_f}{\alpha\tau_{Lf}}. \qquad [24]$$

If the crossing trajectory effect is negligible then the situation of large $\beta\tau_{Lf}$ implies that the particle closely follows the fluid, that $R_f(\theta)$ is the fluid Lagrangian correlation coefficient and that $\epsilon_p = \epsilon_f$, $\overline{v^2} = \overline{u^2}$ and $\alpha\tau_{Lf} = 1$. If v_T/q and $\beta\tau_{Lf}$ are small, the particles will not follow the turbulence. In this limit the particles will be almost stationary and $R_f(\theta)$ equals the Eulerian time correlation $R_{Ef}(\theta)$ measured by an observer moving with the average fluid velocity. In that case $\alpha = (\tau_{Ef})^{-1}$.

Recent theoretical work by Reeks (1977) gives $\tau_{Ef}/\tau_{Lf} = 1$ to 2. His detailed calculations (for $\gamma = 1$) show that τ_f varies smoothly from τ_{Lf} to $1.3\tau_{Lf}$ for decreasing $\beta\tau_{Lf}$ with $v_T/q = 0$. They give $\tau_f \cong \tau_{Lf}$ for $\beta\tau_{Lf} > 2$ and $\tau_f \cong 1.3\tau_{Lf}$ for $\beta\tau_{Lf} < 0.12$.

These results suggest that in the limit of $v_T/q = 0$ that ϵ_p/ϵ_f will only vary from 1.0 to 1.3 as $\beta\tau_{Lf}$ varies from ∞ to 0 even though $\overline{v^2}/\overline{u^2}$ varies from 1 to 0 over this range of $\beta\tau_{Lf}$ (as can be seen from [23]).

The crossing of trajectories has a much greater effect on τ_f than does particle inertia. If $R_{Ef}(x, t)$ is the Eulerian space time correlation in a frame of reference moving with the average fluid velocity, then $R_{Ef}(0, t)$ is the Eulerian time correlation considered above. As pointed out by Yudine (1959) and by Csanady (1963), the correlation coefficient appearing in [20] and [21] for sluggish particles with a large drift velocity can be represented as $R_f(\theta) \cong R_{Ef}(v_T\theta, \theta)$.

In the limit of very large v_T, the particle moves so rapidly through the fluid that $R_f(\theta)$ can be approximated by the Eulerian spatial correlation, $R_{Ef}(v_T\theta, 0)$. For $v_T \to \infty$,

$$\tau_f = \int_0^\infty R_{Ef}(v_T\theta, \theta)\, d\theta \to 0.$$

Table 1. Droplet characteristics and flow conditions ($\rho_p = 1.0$ g/cm^3, $\rho_f = 0.00116$ g/cm^3, $\mu_f = 0.00018$ P)

d_p (μm)	$\bar{U}$ (cm/s)	Re	t (s)	z (cm)	Re_p	u^* (cm/s)	β (s^{-1})	$\beta\tau_{Lf}$	τ^+	v_T (cm/s)	$\bar{V}_0$ (cm/s)	$\frac{v_T}{(\overline{u_r^2})^{1/2}}$
50	1140	36,000	0.043	48.1	0.279	50.5	145	0.836	126	8.4	961	0.21
50	1640	52,000	0.031	48.1	0.279	70.1	162	0.71	245	8.4	1223	0.15
50	1140	36,000	0.183	212.1	0.279	50.5	131	0.737	126	8.4	1126	0.21
50	1640	52,000	0.129	212.1	0.279	50.1	140	0.609	245	8.4	1157	0.15
90	1140	36,000	0.065	77.5	1.106	50.5	50.1	0.287	410	18.5	1223	0.46
90	1640	52,000	0.046	77.5	1.106	70.1	51.4	0.222	790	18.5	1638	0.32
90	1140	36,000	0.183	212.1	1.106	50.5	50.0	0.286	410	18.5	1029	0.46
90	1640	52,000	0.132	212.1	1.106	70.1	54.4	0.236	790	18.5	1096	0.32
150	1140	36,000	0.096	114.0	4.760	50.5	20.4	0.118	1138	47.8	1186	1.20
150	1640	52,000	0.07	114.0	4.760	70.1	19.1	0.082	2211	47.8	1680	0.85
150	1140	36,000	0.179	212.1	4.760	50.5	21.5	0.124	1138	47.8	1186	1.20
150	1640	52,000	0.126	212.1	4.760	70.1	21.2	0.092	2211	47.8	1680	0.85

The calculations performed by Reeks (1977) indicate that "crossing trajectory" effects start to be important for $v_T/q \cong 1$.

RESULTS

Experimental conditions

Table 1 presents a summary of the conditions for all the experiments. Values of τ_{Lf} were obtained from the correlation in Vames & Hanratty (1988) and β was calculated from [2] or [3] using a relative velocity equal to v_T. It is noted that measurements were made at two locations downstream from the injector. Position z_1 was located where deposition on the walls began. As has already been shown by Lee & Hanratty (1988) the droplets that hit the wall do not bounce but form adhering droplets which evaporate. At position $z_2 = 212$ cm the fraction of droplets deposited on the pipe wall was 42, 28 and 10% for 50, 90 and 150 μm droplets, respectively.

The time t was calculated from the initial velocity of the particles $\bar{V}_0$ and z with the equations

$$z = \int_0^t \bar{V}\,dt \qquad [25]$$

and

$$m_p \frac{d\bar{V}}{dt} = \frac{C_D \rho_f}{2}(\bar{U} - \bar{V})^2 A_p, \qquad [26]$$

where $\bar{V}$ and $\bar{U}$ are the time-averaged velocities of the particle and the fluid in the z-direction, and m_p and A_p are the mass and projected area of the particle, respectively. The drag coefficient, C_D, was obtained from Morsi & Alexander (1972). The velocity, V_0, was calculated from an equation derived by Hieftje (1969):

$$V_0 = \frac{4Q}{\pi(0.86d_o)^2}, \qquad [27]$$

where Q is the volumetric flow into the injector and d_o is the orifice diameter.

The calculations of Reeks (1977) suggest that the values of $\beta\tau_f$ are small enough that ϵ_p/ϵ_f would be slightly greater than unity if the crossing trajectory effect were not important. The values of $v_T/(\overline{u_r^2})^{1/2}$ were calculated for the present experiments from measurements of fluid turbulence at $r/R = 0.3$ by Laufer (1954). These indicate that the crossing of trajectories should have been unimportant except for the experiments with 150 μm particles at $\bar{U} = 1140$ cm/s.

Particle trajectories

Individual trajectories, such as shown in figure 3, were analyzed to determine instantaneous values of v_r and v_θ of the particles at different locations in the cross section. The results presented are averages of a number of trajectories within different radial annuli. Because of the tedious methods that were used, the number of trajectories considered was limited. For each of the runs

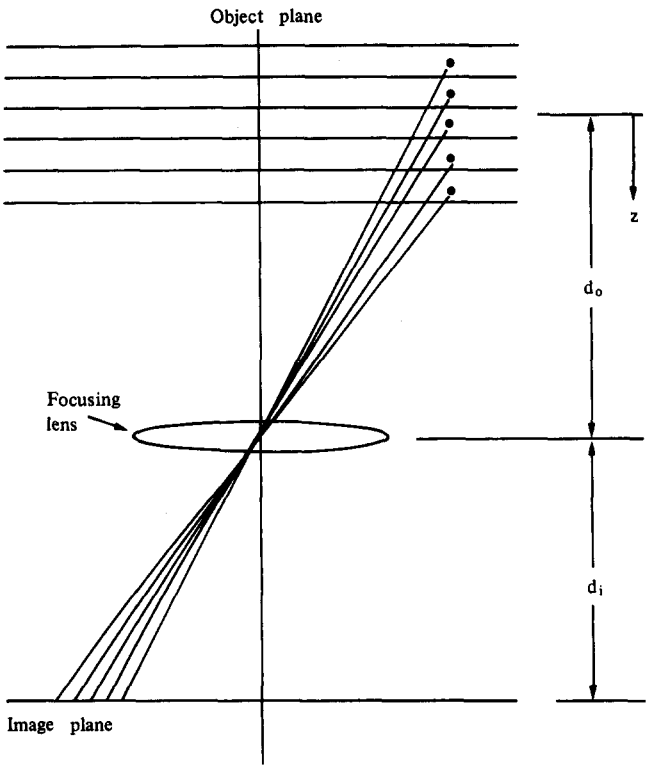

Figure 4. Perspective distortion in optical lens.

listed in table 1, 17–49 photographs were used to analyze 785–911 trajectories. Since the individual trajectories can be considered as random events, the normalized standard error can be calculated from methods given by Bendat & Piersol (1971) as $\epsilon_r = (2/N)^{1/2}$, where N is the number of trajectories. For $N > 800$ the standard error (SE) is $< 5\%$, if one wanted to calculate average values of v_θ, v_r, v_r^2 and v_θ^2 over the whole field of view. For the calculation of profiles, trajectories within a center core and five different annular rings were analyzed. The number in each of these areas would be 160 and the SE would be 11% if an equal number of particles were in each area. This was not the case and statistical error could be larger than this for large r and for the central core.

Figure 5 shows all of the measured trajectories for several of the experiments, after being corrected for error due to perspective. The vectors and, therefore, the velocities are noted to be larger for the 50 μm drops than for the 150 μm drops. This reflects the better ability of the smaller drops to follow the turbulence because of their smaller masses.

Because the droplets are injected in the center of the pipe they initially have a positive radial velocity and a zero tangential velocity. Therefore, for very small z the ratio of the average velocity to the root-mean-square (r.m.s.) velocity, $\bar{v}_r/(\overline{v_r^2})^{1/2}$, approaches unity. Dispersion in this limit is greater for the smaller particles than for the larger particles because it is entirely determined by $\overline{v_r^2}$; i.e. $\epsilon_p = 1/2(\overline{v_r^2})t$. The smaller particles are thus observed to reach the wall at a smaller z because of their larger velocity. The period over which the influence of the initial trajectory persists is much longer for the larger 150 μm particles.

A close examination of the vectors in figure 5 for the smaller z reveals that the droplets have a preferential flow in the $+r$-direction. Vector diagrams such as this for 150 μm particles at $z = 48.1$ cm would show an even more persistent motion in the $+r$-direction than indicated for the 50 μm drops, as would be expected because of their larger mass.

It is noted that at 212.1 cm downstream all of the particles show a haphazard motion, indicating a diffusional mechanism for the dispersion of the droplets.

Particle velocities

Measurements of the average θ-component of the velocity, $\bar{v}_\theta$, give a value of zero, which indicates the absence of a large-scale swirling motion. Measurements of the r-component, $\bar{v}_r$, are plotted in figures 6 and 7. Averages were calculated over annular regions bounded by $r = 0.2$, 0.4,

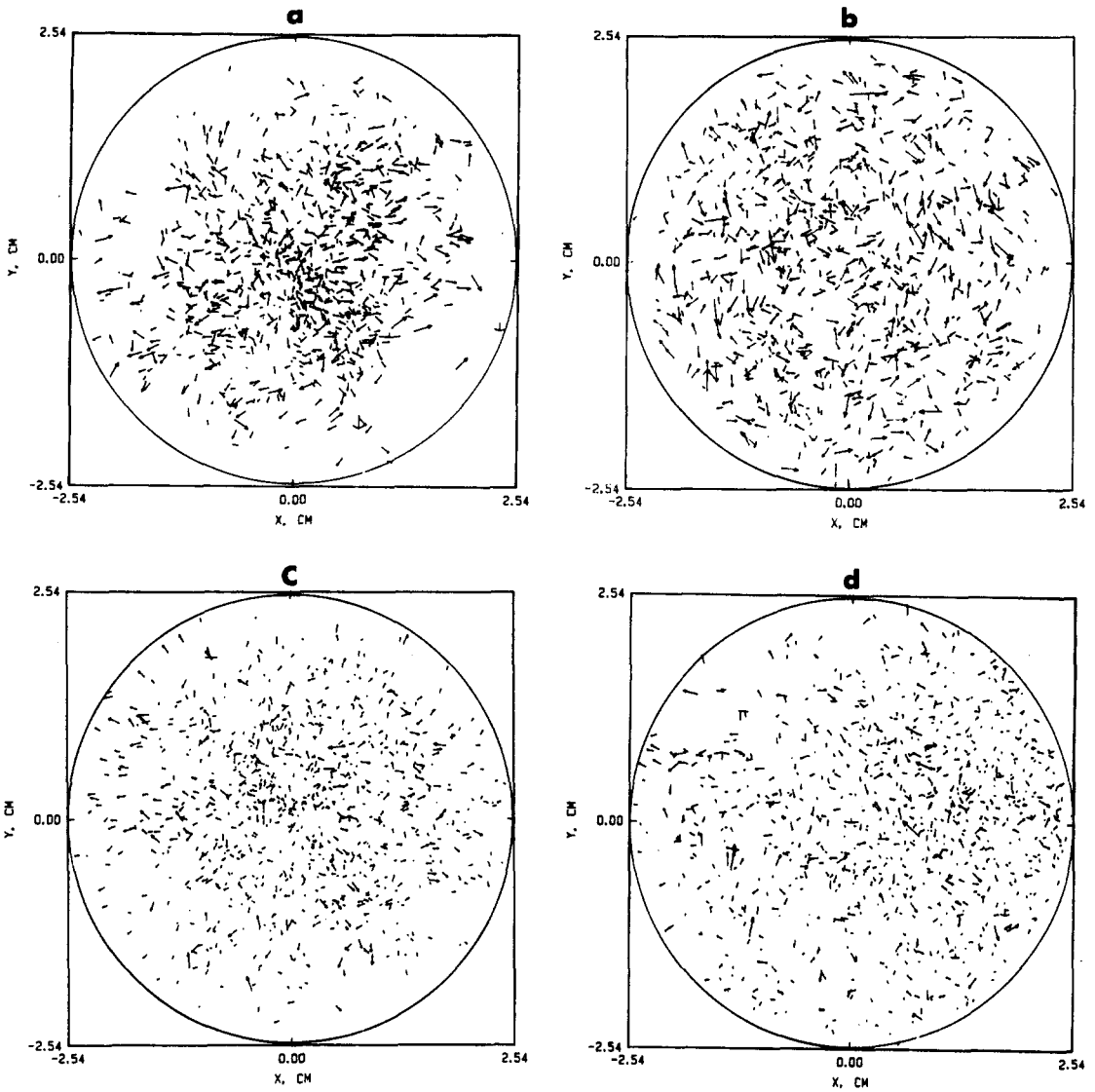

Figure 5. Droplet trajectories at Re = 52,000 for: (a) 50 μm droplets at $z = 48.1$ cm; (b) 50 μm droplets at $z = 212.1$ cm; (c) 150 μm droplets at $z = 114.0$ cm; (d) 150 μm droplets at $z = 212.1$ cm.

0.6, 0.8 and 1.0. The values indicated at $r = 0.1$ are, thus, an average over the central disk of radius 0.2. Non-zero vales of $\bar{v}_r$ are indicative of dispersion toward the wall and should be considered as a measure of the flux defined by [4]. The value depends on the magnitude of $\overline{v_r^2}$ and on the fraction of the droplets which are moving in the $+r$-direction. Therefore, they need not be different for the different drop sizes. In fact, it is noted that they are of the same magnitude at $z = 212.1$ cm, where a diffusion-type mechanism is operative. This is because the diffusivities for the three drop sizes are roughly the same even though the turbulent velocities are quite different.

Meaurements of $(\overline{v_r^2})^{1/2}$ and $(\overline{v_\theta^2})^{1/2}$ are given in figures 8–10. It is noted that the $(\overline{v_r^2})^{1/2}$ is the same at z_1 and z_2, but that $(\overline{v_\theta^2})^{1/2}$ is greater at z_2 than at z_1. The greater time required for the θ-intensities to reach stationary values is probably associated with the use of a centrally located injector for which particles are initially entrained into the turbulence with a positive v_r and a zero v_θ. The $(\overline{v_\theta^2})^{1/2}$ profile for 50 μm drops shows an increase with increasing r, as do the data for fluid turbulence $(\overline{u_\theta^2})^{1/2}$. All the other data, however, show small variation with radial position.

A comparison of the measurements of particle turbulence for $r/R \leqslant 0.4$ with the fluid turbulence is given in columns 6 and 7 of table 2. It is noted that the mean-squares of the particle turbulent velocities for all three drop sizes are much lower than the mean-squares of the fluid turbulent velocity fluctuations, and that the difference increases with increasing drop size. Values of $(\overline{v_r^2})^{1/2}$

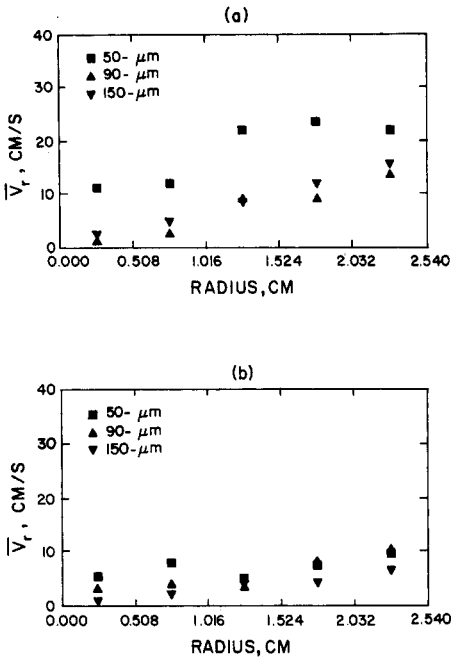

Figure 6. The effect of drop size on $\bar{v}_r$ at Re = 36,000: (a) z_1; (b) z_2.

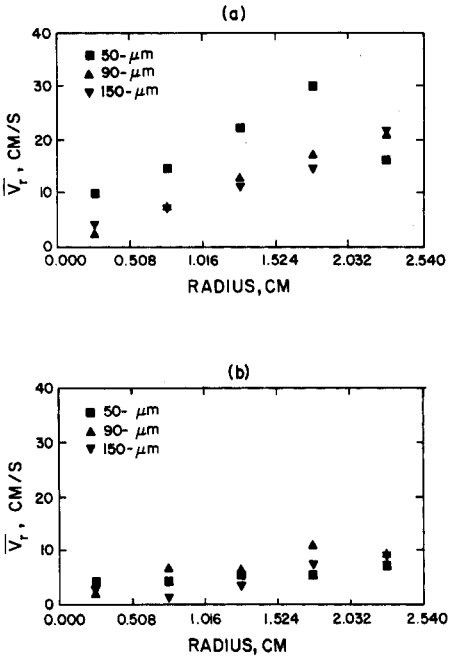

Figure 7. The effect of drop size on $\bar{v}_r$ at Re = 52,000: (a) z_1; (b) z_2.

estimated by Vames & Hanratty (1988) for the central region of a pipe from dispersion measurements are also given. Approximate agreement is noted.

As can be seen from table 1, increasing drop size corresponds to decreasing $\beta\tau_{Lf}$. The ratio of the particle and fluid turbulence is plotted against $\beta\tau_{Lf}$ in figure 11. The curves through the data are [23] with $\alpha\tau_{Lf} = 0.7$ for the r-velocities and $\alpha\tau_{Lf} = 0.8$ for the θ-velocities. This gives a value of

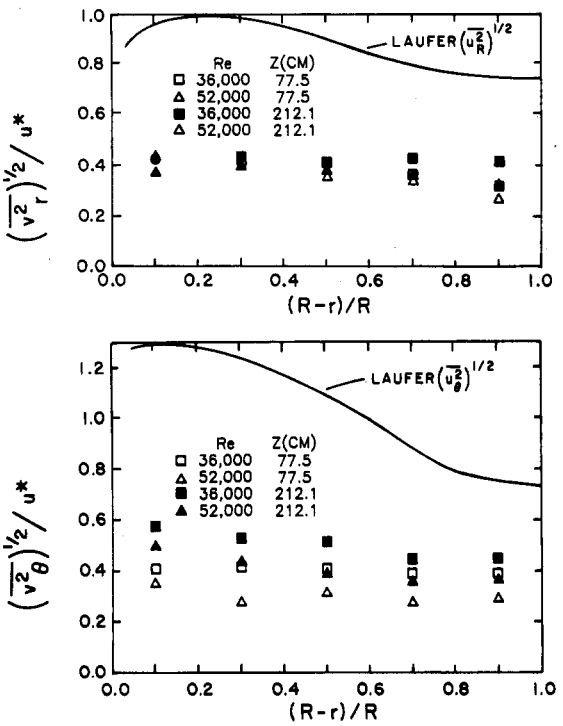

Figure 8. The effects of Re and axial distance on the r.m.s. intensity normalized with the friction velocity for the 50 μm droplets.

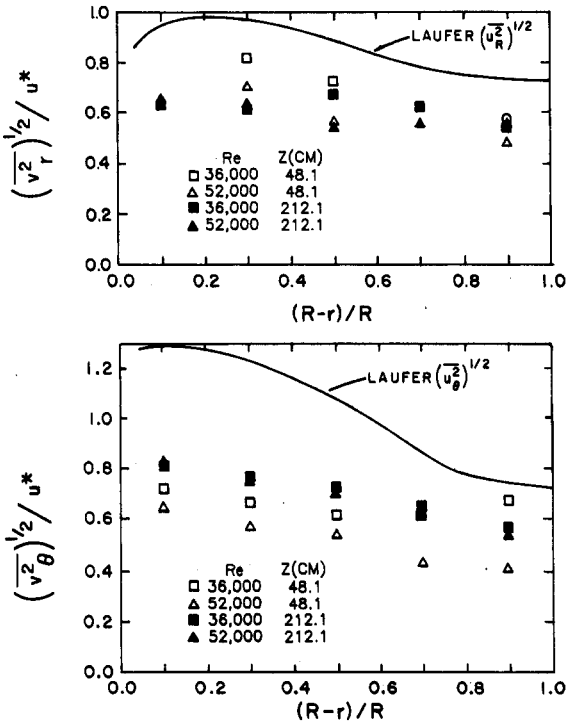

Figure 9. The effects of Re and axial distance on the r.m.s. intensity normalized with the friction velocity for the 90 μm droplets.

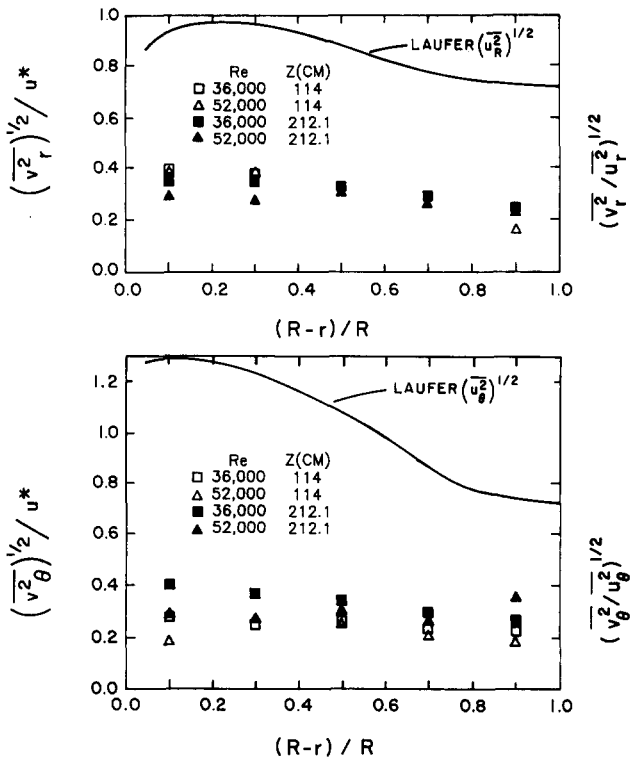

Figure 10. The effects of Re and axial distance on the r.m.s. intensity normalized with the friction velocity for the 150 μm droplets.

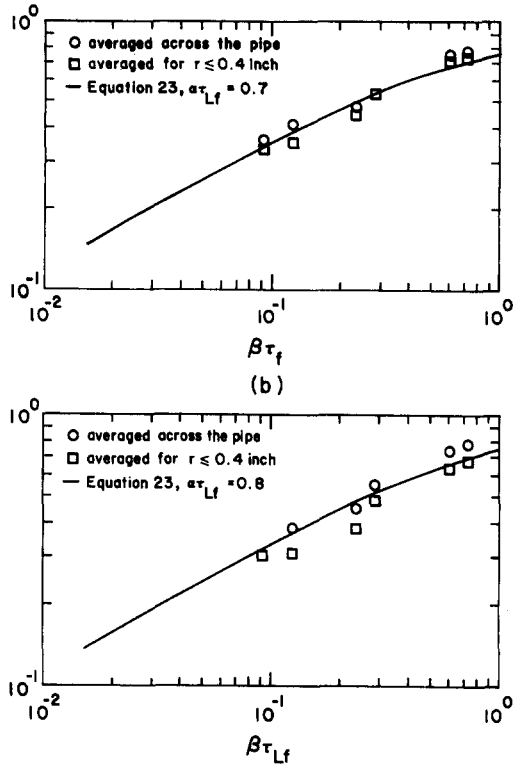

Figure 11. Experimental values and predictions of [44] and [45] for the ratio of the intensities as a function of $\beta\tau_f$ at z_2: (a) radial direction; (b) tangential direction.

the ratio of the time scale characterizing $R_f(\theta)$ to the Lagrangian time scale of about 1.3. This number seems reasonable if the crossing trajectory effect is small.

Particle diffusivities

Eulerian diffusion coefficients can be calculated from measurements of the average velocities by using [4] and [5]:

$$\epsilon_p(r) = \bar{v}_r \frac{\bar{C}}{\left(-\frac{d\bar{C}}{dr}\right)}. \qquad [28]$$

Table 2. Comparison of turbulence intensities

d_p (μm)	Re	z (cm)	$\frac{(v_r^2)^{1/2}}{(u_r^2)^{1/2}}$ (av. over the whole cross section)	$\frac{(v_\theta^2)^{1/2}}{(u_\theta^2)^{1/2}}$ (av. over the whole cross section)	$\frac{(v_r^2)^{1/2}}{(u_r^2)^{1/2}}$ (av. over $r \leq 0.4R$")	$\frac{(v_\theta^2)^{1/2}}{(u_\theta^2)^{1/2}}$ (av. over $r \leq 0.4R$")	$\frac{(v_r^2)^{1/2}}{(u_r^2)^{1/2}}$ (Vames & Hanratty 1988)
50	36,000	48.1	0.85	0.69	0.75	0.69	0.63
50	52,000	48.1	0.74	0.52	0.68	0.44	0.64
90	36,000	77.5	0.49	0.44	0.44	0.43	0.52
90	52,000	77.5	0.48	0.31	0.41	0.30	0.52
150	36,000	114.0	0.41	0.27	0.34	0.25	0.23
150	52,000	114.0	0.39	0.25	0.30	0.22	0.26
50	36,000	212.1	0.77	0.78	0.74	0.67	
50	52,000	212.1	0.75	0.74	0.71	0.63	
90	36,000	212.1	0.53	0.55	0.53	0.48	
90	52,000	212.1	0.48	0.45	0.45	0.38	
150	36,000	212.1	0.41	0.38	0.35	0.31	
150	52,000	212.1	0.36	0.30	0.33	0.30	

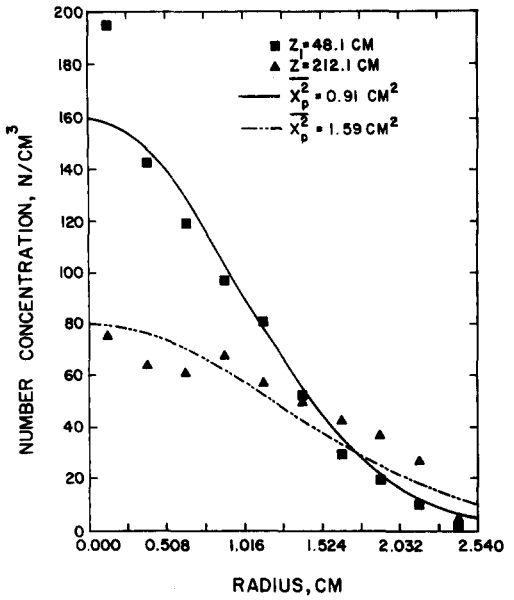

Figure 12. Number concentration distribution for 50 μm droplets at Re = 52,000.

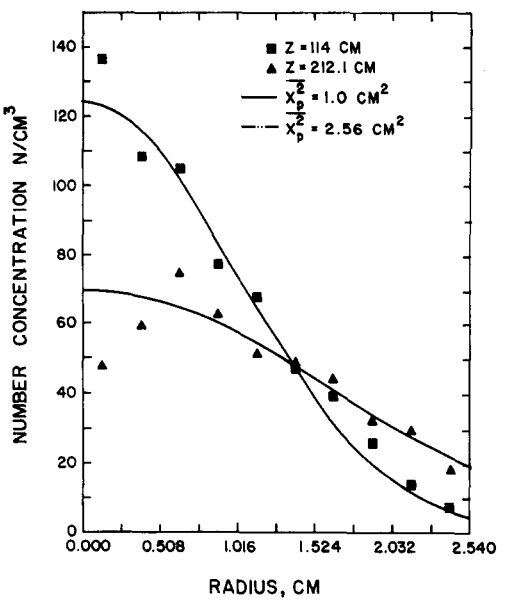

Figure 13. Number concentration distribution for 150 μm droplets at Re = 52,000.

To evaluate the ratio of the concentration and the concentration gradient the photographs were divided into ten equal radial increments. The number concentration of droplets in a radial increment was calculated from

$$\bar{C} = \frac{N}{\pi(r_{i+1}^2 - r_i^2)\,\Delta z n}, \qquad [29]$$

where N is the total number of images in the annulus between r_i and r_{i+1}, Δz is the thickness of the individual light sheets and n is the number of light sheets. Results for 50 and 150 μm drops at a gas Re of 52,000 are presented in figures 12 and 13.

The main focus of the initial experiments was to get good average values of $\overline{v_r^2}$ and $\overline{v_\theta^2}$ over the pipe cross section. The size of the samples required to do this was not large enough to get precise concentration profiles or a very precise measure of the variation of $\bar{v}_r$ with radius. This is reflected in the scatter of the data in figures 12 and 13. In order to obtain an estimate of ϵ_p these concentration profiles were fitted with Gaussian curves, as shown in the figures. Comparisons of values of $\overline{X_p^2}$ obtained from these fits are in good agreement with the measurements of Vames & Hanratty (1988).

A simple average fit to most of the measurements of $\bar{v}_r$, shown in figures 6 and 7, is

$$\bar{v}_r = kr. \qquad [30]$$

If the concentration profile can be fitted with a Gaussian curve then [28] and [30] give a constant value of ϵ_p at a given location downstream of the injector:

$$\epsilon_p = \frac{\bar{v}_r \overline{X_p^2}}{r} = k\overline{X_p^2}. \qquad [31]$$

The values of ϵ_p obtained in this way are presented in table 3. They were calculated from [31] only for the runs at z_1 where a small fraction of the drops had deposited and where a comparison could be made with the $\overline{X_p^2}$ values of Vames & Hanratty (1988). The runs with the 50 μm drops were not considered because it was very difficult to fit the measurements of $\bar{v}_r(r)$ with a linear relation.

The values of ϵ_p calculated in this way are compared in table 3 with values of ϵ_f obtained from measurements of the dispersion of marked fluid elements in pipe flows by Towle & Sherwood

Table 3. Estimates of the diffusion coefficient

d_p (μm)	Re	z (cm)	$\overline{X_p^2}$ (measured)	$\overline{X_p^2}$ (Vames & Hanratty 1988)	ϵ_p (cm^2/s)	ϵ_f (cm^2/s)	$\frac{\epsilon_p}{\epsilon_f}$
50	36,000	48.1	0.8	0.8			
50	52,000	48.1	0.91	0.91			
90	36,000	77.5	1.4	1.37	8.4	9.5	0.88
90	52,000	77.5	1.4	1.34	13.4	13.1	1.02
150	36,000	114.0	1.32	0.86	5.9	9.5	0.62
150	52,000	114.0	1.0	0.91	8.9	13.1	0.68

(1939), Boothroyd (1967), Groenhof (1970) and Taylor & Middleman (1974). They are represented over the Re range 10,000–100,000 by the equation

$$\frac{\epsilon_f}{u^* 2R} = 0.037. \qquad [32]$$

It is noted that the estimated values of ϵ_p/ϵ_f for the 90 μm drops are close to unity even though the turbulent velocity fluctuations of particles were found to be much smaller than the turbulent velocity fluctuations of the fluid. The estimated value of ϵ_p/ϵ_f for the 150 μm at Re = 52,000 is significantly smaller than unity. This could be explained as being associated with the large value of the terminal velocity for this run (see table 1).

DISCUSSION AND CONCLUSIONS

The axial viewing technique

The axial viewing photographic technique described in this paper offers the opportunity to obtain much needed information about the turbulence characteristics of particles. The use of multiple images allowed for an accurate definition of the distance travelled. However, for very small distances these multiple images appeared as a streak and it was difficult to determine the number of images (or the time interval) defining the streak. This particularly affected the accuracy of measurements of $\bar{v}_r$ at small r. Recent experiments at the University of Illinois by Young (1988) have revealed that this difficulty can be avoided by color coding the flashes.

In the initial experiments with this technique emphasis was placed on obtaining average values over the pipe cross section of the mean-square of the r- and θ-components of the turbulent velocity fluctuations. This required a smaller number of photographs (sample size) than the determination of turbulent diffusivities. As a result, these initial measurements do not provide the type of precise determinations needed to define unequivocally the effect of $\beta\tau_{Lf}$ and of $v_T^2/\overline{u_r^2}$ on turbulent diffusion. Nevertheless, some important results have been obtained.

Particle velocities

They provide the first measurements of $\overline{v_\theta^2}$ and the first direct measurements of particle flux, $\bar{v}_r$. The values of $\overline{v_\theta^2}$ and $\overline{v_r^2}$ are found to be much smaller than those of the fluid turbulent velocity fluctuations. Over the range of $\beta\tau_{Lf}$ studied ($\beta\tau_{Lf} = 0.1$ to 0.8) these measurements are represented by [23] with $\alpha\tau_{Lf} = 0.7$. This is reasonable, since it indicates that the time scale of the fluid velocity fluctuations seen by the particles is approx. 30% larger than the Lagrangian fluid time scale.

Particle diffusivities

The approximate measurements show that ϵ_p is close to ϵ_f, even though the turbulent velocity fluctuations are much smaller than the fluid velocity fluctuations, provided $v_T/(\overline{v_r^2})^{1/2} < 0.85$.

A value of $\epsilon_p/\epsilon_f = 0.68$ is estimated for a run characterized by $\beta\tau_{Lf} = 0.082$ and by $v_T/(\overline{v_r^2})^{1/2} = 0.85$. This smaller value of ϵ_p/ϵ_f could result from the particles not being in the field long enough to have reached their long-time behavior or from Yudine's "crossing trajectories" effect. However, a rough estimate of ϵ_p from the measurements for the 150 μm drops at $z = 212.1$ cm, where considerable deposition had occurred, gives $\epsilon_p/\epsilon_f \cong 0.75$. Therefore, the tentative conclusion is reached that the crossing of trajectories could start to cause ϵ_p to be significantly lower that ϵ_f at $v_T/(\overline{v_r^2})^{1/2} \cong 0.85$.

The results are consistent with the calculation of Reeks (1977) which was performed for a homogeneous isotropic turbulent field and for a particular assumed form for the wavenumber–frequency spectrum. In fact, direct comparisons can be made with his figures 4, 6 and 7 if his velocity parameter and wavenumber are represented by the equations

$$u_0 = 0.8u^* \quad [33]$$

and

$$0.9\frac{v_0}{k_0} = 0.037(u^*2R). \quad [34]$$

The preliminary results with the axial view photographic technique thus suggest that future work should focus on defining exactly how $v_T/(\overline{u^2})^{1/2}$ is affecting ϵ_p.

Lift force

Finally, some comment should be made about possible effects of the Saffman lift force considred by a number of authors. The usual practice in estimating this effect is to assume the particle, on average, sees a fluid velocity gradient equal to the time-averaged value. Such an approach would indicate that a significant fraction of the $\bar{v}_r$ values for 150 μm particles shown in figures 6 and 7 is due to lift.

However, no corrections were made because of uncertainties in the use of this correction. The principal problem is that the Saffman analysis was made for a laminar flow. In a turbulent field the particle is entrained in a fluid region in which the velocity gradient could be much smaller than the time averaged velocity gradient. In fact, recent work by Young (1988) indicates that outside the viscous wall region the effect of Saffman lift forces can be neglected.

Acknowledgements—This work has been supported by the National Science Foundation under Grant NSF CBT 85-19098, by the Department of Energy under Grant DEF G02-86ER13556 and by the Shell Companies Foundation.

REFERENCES

ARNOLD, C. R. & HEWITT, G. F. 1967 Further developments in the photography of two-phase gas–liquid flow. UKAEA Report AERE-R 5318.

BENDAT, J. S. & PIERSOL, A. G. 1971 *Random Data: Analysis and Measurement Procedure.* Wiley, New York.

BOOTHROYD, R. G. 1967 Turbulence characteristics of the gaseous phase in duct flow of a suspension of fine particles. *Trans. Instn chem. Engrs* **45,** T297.

CSANADY, G. T. 1963 Turbulent diffusion of heavy particles in the atmosphere. *J. atmos. Sci.* **20,** 201–208.

FRIEDLANDER, S. K. 1957 Behavior of suspended particles in a turbulent fluid. *AIChE Jl* **3,** 381.

FRIEDLANDER, S. K. & JOHNSTONE, H. F. 1957 Deposition of suspended particles from turbulent gas streams. *Ind. Engng Chem.* **49,** 1151–1156.

GANIC, E. N. & MASTANAIAH, K. 1981 Investigation of droplet deposition from a turbulent gas stream. *Int. J. Multiphase Flow* **7,** 401–422.

GROENHOF, H. C. 1970 Eddy diffusion in the central region of turbulent flows in pipes and between parallel plates. *Chem. Engng Sci.* **25,** 1005 (1970).

HEWITT, G. F. & ROBERTS, D. N. 1969 Investigation of interfacial phenomena in annular two-phase flow by means of the axial view techniques. UKAEA Report AERE-R 6070.

HIEFTJE, G. M. 1969 Investigation into flame spectrometric processes and methods using an isolated droplet technique. Ph.D. Thesis, Univ. of Illinois, Urbana.

HUTCHINSON, P., HEWITT, G. F. & DUKLER, A. E. 1971 Deposition of liquid or solid dispersions from gas streams: a stochastic model. *Chem. Engng Sci.* **26,** 419–439.

LAUFER, J. 1954 The structure of turbulent fully developed flow. NACA Report No. 1174.

LEE, M. M. 1984 Droplet dispersion in vertical turbulent pipe flow. M.S. Thesis, Univ. of Illnois, Urbana-Champaign.

LEE, M. M. & HANRATTY, T. J. 1988 The inhibition of droplet deposition by the presence of a liquid wall film. *Int. J. Multiphase Flow* **14,** 129–140.

MCCOY, D. D. & HANRATTY, T. J. 1977 Rate of deposition of droplets in annular two-phase flow. *Int. J. Multiphase Flow* **3,** 319–331.

MORSI, S. A. & ALEXANDER, A. J. 1972 An investigation of particles trajectories in two-phase flow systems. *J. Fluid Mech.* **55,** 193.

REEKS, M. W. 1977 On the dispersion of small particles suspended in an isotropic turbulent fluid. *J. Fluid Mech.* **83,** 529.

TAYLOR, A. R. & MIDDLEMAN, S. 1974 Turbulent dispersion in drag reducing fluids. *AIChE Jl* **20,** 454.

TOWLE, W. L. & SHERWOOD, T. K. 1939 Mass transfer in the central portion of a turbulent air stream. *Ind. Engng Chem.* **31,** 457.

VAMES, J. S. & HANRATTY, T. J. 1988 Turbulent dispersion of droplets for air flow in a pipe. *Expts Fluids* **6,** 94–104.

YOUNG, J. B. 1988 An experimental study of solid particle motion in a turbulent liquid pipe flow. Ph.D. Thesis, Univ. of Illinois, Urbana.

YUDINE, M. I. 1959 Physical considerations on heavy-particle diffusion. In *Atmospheric Diffusion and Air Pollution*; *Advances in Geophysics*, Vol. 6, p. 185. Academic Press, New York.